AIAA JOURNAL
Vol. 50, No. 12, December 2012

Aeroacoustic Performance of Fractal Spoilers

J. Nedić,* B. Ganapathisubramani,† and J. C. Vassilicos‡
Imperial College London, London, England SW7 2AZ, United Kingdom
and
J. Borée,§ L. E. Brizzi,§ and A. Spohn¶
Universite de Poitiers, Futuroscope Chasseneuil 86961, France

DOI: 10.2514/1.J051387

One of the major environmental problems facing the aviation industry is that of aircraft noise. The work presented in this paper, done as part of the European Union's Optimisation for Low Environmental Noise Impact Project, looks at reducing spoiler noise while maintaining aerodynamic performance, through means of large-scale fractal porosity. It is hypothesized that the highly turbulent flow generated by fractal grids from the way the multiple-length scales are organized in space, would reduce the impact of the recirculation region and, with it, the low-frequency noise it generates. In its place, a higher frequency noise is introduced, which is more susceptible to atmospheric attenuation and is less offensive to the human ear. A total of nine laboratory-scaled spoilers were looked at, seven of which had a fractal design, one with a regular grid design, and one solid for reference. The spoilers were inclined at an angle of 30 deg. Force, acoustic, and flow visualization experiments on a flat plate were carried out and it was found that the present fractal spoilers reduce the low-frequency noise by 2.5 dB. Results show that it is possible to improve the acoustic performance by modifying a number of parameters defining the fractal spoiler, some of them very sensitively. From these experiments, two fractal spoilers were chosen for a detailed aeroacoustic study on a three-element wing system, where it was found that the fractal spoilers had a reduction of up to 4 dB in the sound pressure level, while maintaining similar aerodynamic performances as conventional solid spoilers on the measured wing system.

Nomenclature

B_L	=	mean length of recirculating flow region/bubble, mm
C_D	=	coefficient of drag
C_L	=	coefficient of lift
D	=	drag force, N
L	=	lift force, N
L_0	=	maximum bar length in fractal grid, mm
M	=	Mach number
M_{eff}	=	effective mesh size of fractal grids, mm
M_g	=	mesh size of regular grids, mm
N	=	number of fractal iterations
P	=	measured rms pressure, Pa
P_D	=	percentage change in drag force compared with solid spoiler, %
P_L	=	percentage change in lift force compared with solid spoiler, %
P_σ	=	percentage change in blockage ratio compared with solid spoiler, %
P_0	=	reference acoustic pressure, Pa
Re_{t_0}	=	Reynolds number based on maximum lateral bar thickness in fractal grid
R_L	=	ratio of the successive bar lengths
R_t	=	ratio of successive bar thicknesses
T_H	=	length of spoiler, mm
T_V	=	height of spoiler, mm
t_r	=	ratio between the lateral thickness of the thickest and thinnest bars
t_0	=	maximum lateral bar thickness in fractal grid, mm
U	=	time-averaged streamwise velocity, ms^{-1}
U_∞	=	freestream velocity, ms^{-1}
u	=	instantaneous streamwise velocity, ms^{-1}
u'	=	fluctuating streamwise velocity, ms^{-1}
V	=	time-averaged streamwise velocity, ms^{-1}
v	=	instantaneous wall normal velocity, ms^{-1}
v'	=	fluctuating streamwise velocity, ms^{-1}
W	=	time-averaged streamwise velocity, ms^{-1}
w	=	instantaneous spanwise velocity, ms^{-1}
w'	=	fluctuating streamwise velocity, ms^{-1}
X	=	streamwise plane
x	=	streamwise distance, mm
x_{peak}	=	location of peak turbulence intensity behind grid, m
Y	=	wall normal plane
y	=	wall normal distance, mm
Z	=	spanwise plane
z	=	spanwise distance, mm
α	=	angle of attack, deg
ϵ	=	porosity of spoiler, open area divided by total area
σ	=	blockage ratio of spoiler, solid area divided by total area
σ_B	=	normalized area of recirculating flow region
σ_g	=	blockage ratio of grids
ϕ	=	polar angle, deg

Presented at the 49th AIAA Aerospace Sciences Meeting including the New Horizons Forum and Aerospace Exposition, Orlando, Florida, 4–7 January 2011; received 1 June 2011; revision received 8 November 2011; accepted for publication 9 February 2012.

*Ph.D. Student, Department of Aeronautics, Imperial College London. AIAA Member

†Lecturer, Department of Aeronautics, Imperial College London; currently Professor, Aerodynamics and Flight Mechanics Group, School of Engineering Sciences, University of Southampton, Highfield, Southampton SO17 1BJ. AIAA Member.

‡Professor, Department of Aeronautics, Imperial College London.

§Professor, Département Fluide, Thermique et Combustion, Institut Prime, BP 40109, Futuroscope Chasseneuil 86961.

¶Lecturer, Département Fluide, Thermique et Combustion, Institut Prime, BP 40109, Futuroscope Chasseneuil 86961.

I. Introduction

A VARIETY of natural systems are found to exhibit rough or fragmented geometric shapes that can be subdivided in parts, each of which is at least approximately a reduced-size copy of the whole, known as fractal patterns. Therefore, many geological, environmental, and biological flow systems can be seen as flows past fractal or multiscale objects. Such flows pose a formidable challenge to researchers due to complex geometries and the presence of

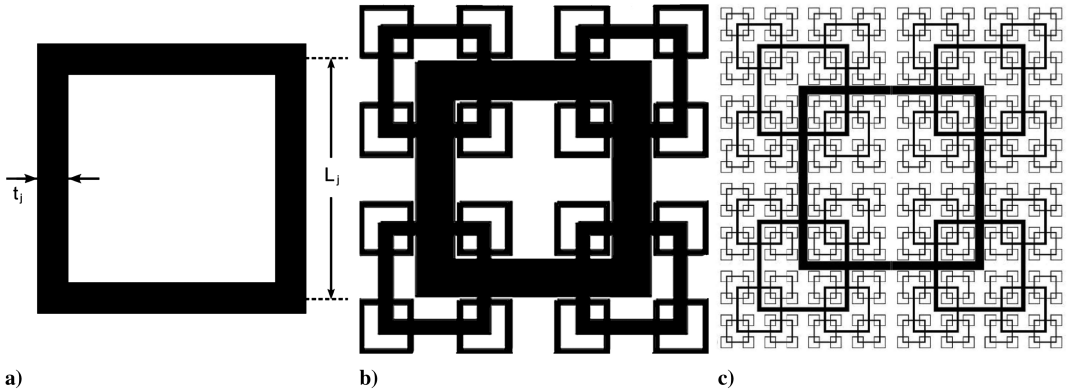

Fig. 1 Examples of fractal square grids with definition of dimensions.

a multitude of length scales in the very system generating the turbulent flow.

Over the last decade, the nature of fractal-generated turbulence has been studied, both experimentally [1–5] and computationally [6–8], with recent papers suggesting that a new class of turbulence should be defined [9]. Research has shown that fractal-grid-generated turbulence exhibits a unique quality that regular grids do not; they introduce a variety of length scales into the flow.

Aircraft noise is becoming a growing area of study within the aviation industry, with the general aim being to reduce the noise without affecting the aerodynamic characteristics of the aircraft. The study by Sakaliyski et al. [10] had already looked into the acoustic performance of perforated plates, however, the introduction of multiple length scales from the fractal grids could lead to step-change improvements. The work presented in this paper looks at exactly that. In Sec. II, we present a review of past work on fractal-generated flows as well as past and present design of low-noise spoilers. Section III covers a parametric study of the acoustics and aerodynamics of several wall-mounted spoilers, both with fractal patterns, regular grids, and a solid one for comparison. In Sec. IV, the aeroacoustics of two wing-mounted fractal spoilers are presented.

II. Literature Review and Spoiler Design

A. Fractal-Generated Turbulence

Initial studies of fractal-generated turbulence looked at three-dimensional fractal objects to generate turbulence [1,2], however, further studies by Hurst and Vassilicos [3], Seoud and Vassilicos [4], and Mazellier and Vassilicos [5], used planar fractal grids that can easily be placed in a wind-tunnel test section. Whereas a regular grid will effectively introduce a single length scale into the flow, namely, the mesh size, a fractal grid can, in principle, introduce a wide range of length scales into the flow (see Fig. 1). In practice, the number of length scales in a fractal grid is limited by the constraints of the tunnel, that is, the cross-sectional area, as well as machining constraints. It is the introduction of these varying length scales, organized in a particular way in space, and the associated wakes/jets/eddies and their interactions, that produce a unique turbulent flow, which has a large production region, higher turbulence intensity, and higher Reynolds numbers over a much wider spatial extent than regular grids with higher blockage ratio σ and at the same flow rate (blockage ratio is defined as the ratio between solid area and total area). Note that due to the various length scales associated with fractal grids, many Reynolds numbers can be defined.

Hurst and Vassilicos [3] focused on a total of 21 fractal grids, split into three shape families: cross grids, *I* grids, and space-filling fractal square grids. Each family had seven grids of varying thicknesses and lengths. The turbulence generated by the space-filling fractal square grids exhibited very clearly a protracted region of turbulence production, with a peak in turbulence intensity being reached at a certain distance x_{peak} downstream. Subsequently, Mazellier and Vassilicos [5] provided the most up-to-date relationship between the grid geometry and x_{peak} along the centerline, shown in Eq. (1), where t_0 is the maximum lateral bar thickness and L_0 is the maximum bar length on the fractal grid (see Fig. 1):

$$x_{\text{peak}} = 0.45\frac{L_0^2}{t_0} \tag{1}$$

This equation was established [5] for space-filling fractal square grids with 25% blockage and at least $N = 4$ fractal iterations, similar to the grid seen in Fig. 1c and a value of the thickness ratio t_r (ratio between the lateral thickness of the thickest to the thinnest bars) that is not too small.

Hurst and Vassilicos [3] found that best homogeneity of the turbulent flows generated by fractal grids was observed for increasing thickness ratio t_r, which can also lead to increasing turbulence intensity and Reynolds number. Of all the grids studied, the space-filling fractal square grids were the most promising and, since then, research has focused on this family of grids.

B. Aircraft and Spoiler Noise

In general, there are two main sources of noise on a typical aircraft: engine (split into fan intake and exhaust, combustion, turbine, and jet noise) and the airframe. Owens [11] looked at the contribution from each of these sources to the overall noise of the aircraft, the results of which can be seen in Fig. 2. From this, the engine is by far the dominant noise source on the aircraft at takeoff, and the airframe noise only becomes relevant as the aircraft comes in to land. It is here that all slats, flaps, and spoilers are deployed to allow for steep approach paths and reduced landing speed, contributing to about 26% of the total noise of the airborne aircraft; thereby the spoilers increase drag and reduce lift.

Over the past several decades, research has looked at understanding and reducing jet noise [12–15] and airframe noise [10,16–19]. This study focuses on spoiler noise. A spoiler, which is deployed to reduce the lift on the aircraft, generates a low-frequency noise due to the large-scale wall-bound flow that is formed behind it: the recirculation bubble. This low-frequency noise is less susceptible to atmospheric attenuation and can travel a lot further than high-frequency noise, which means that low-frequency noise sources are a problem on aircraft as they can affect the environment close to an airport. Therefore, reducing this low-frequency noise is a priority for the aviation industry.

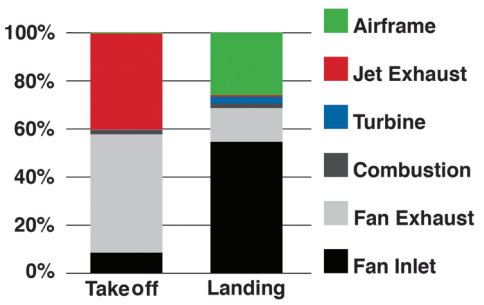

Fig. 2 Contribution of total aircraft noise at takeoff and landing according to Owens [11].

C. Porous Fences and Spoilers

There have been several studies looking at the effect of blockage ratio σ on two-dimensional plates, or fences, over the last few decades. The most prominent of these was by Castro [20]. Depending on blockage ratio, Castro demonstrated experimentally that two well-distinguishable flow regimes exist. For plates with high blockage ratio, a detached recirculation bubble is observed. As the blockage ratio decreases, more bleed air is allowed to pass, resulting in the recirculation region moving further downstream until, at a certain blockage, it disappears all together. The coefficients of drag for these fences were also obtained from wake and force balance measurements, which showed a distinct increase in drag coefficient C_D as the blockage ratio increased from 70% to 80%, suggesting that at some point in this range, the bleed air is not allowing the flow to come around to create the recirculating region.

Similar experiments were later carried out by Ranga Raju et al. [21], Shiau [22], and Lee and Kim [23] who all studied the flow past porous fences, in particular looking at the turbulent characteristics and the streamwise evolution of the flow. Again, the recirculation region was found to exist up to a certain porosity, $\epsilon = 20\%$ ($\sigma = 80\%$) in the case of Lee and Kim, and two distinct peaks exist in the streamwise turbulence intensity profiles: one in the region behind the fence and another in the freestream. Fang and Wang [24] performed large-eddy simulations to study the flow past porous fences, also noticing a detached recirculation region, however, in their simulations, the region did not disappear as the porosity increased.

Sakaliyski et al. [10] showed that a perforated plate placed perpendicular to, and subjected to, a three-dimensional flow, introduced bleed flow with smaller length scales and, as such, had a higher frequency noise signature. They first of all point out that "conventional spoilers create drag in a noisy manner involving unsteady wakes which inevitably generate noise at low frequencies," and theorized that the large-scale flow that exists behind a solid spoiler would be broken down and thus the predominant contribution to the noise would come from the "turbulent mixing and surface interaction." This theory is based on previous studies by Tam et al. [13,14], in which it was found that jets, such as those coming through porous plates, have a higher peak acoustic frequency. As a result, the noise would shift to higher frequencies, which are deemed less annoying to the human ear. Sakaliyski et al. [10] claimed that the spoiler with a blockage ratio of 75% gave the optimum acoustic performance.

D. Fractal Spoilers

1. Fundamental Considerations

Unlike regular grids and even porous plates, space-filling fractal square grids, such as the one seen in Fig. 1, are capable of introducing a variety of length scales into the flow in a spatially organized fashion. Hurst and Vassilicos [3] and Mazellier and Vassilicos [5] identified two main differences between the flows generated by a regular grid and a fractal square grid; the turbulence intensity peaks much further downstream in the latter case and is a function of the thickness ratio t_r, which we can tune at will while keeping other parameters, such as the blockage ratio, constant. This gives us a type of porosity with much greater possibilities to disrupt the creation and the dynamics of the recirculation zone, thus influencing noise, particularly at the low frequencies.

It is hypothesized that the fractal-generated, high-intensity turbulent flow with its spatially organized multilength scales would not only mimic but even significantly improve the results of a more porous plate in that the recirculation region is removed entirely and, with it, the low-frequency noise. This view is based on the fractal spoilers being able to create a more intense turbulent flow, with an increased level of fluctuating momentum behind the spoiler that would result in an increased level of interaction with the recirculation region. It is, however, important to note that the highly two-dimensional experiments done by Castro [20] and the three-dimensional nature of the flow around aircraft spoilers would give different results. Similarly, one should note that Castro's plates were perpendicular to the flow, whereas our spoilers are inclined at 30 deg to the horizontal.

As well as reducing the noise signature, the spoilers must also retain their aerodynamic performance, which is essential for integration onto the aircraft. Acoustic measurements such as those done by Sakaliyski et al. [10] are therefore not sufficient to select the spoiler. For this reason, we completed our study by obtaining lift and drag measurements to verify their aerodynamic performances.

2. Spoiler Configuration

A total of nine spoilers were manufactured, seven of which had a fractal design with three fractal iterations, one was designed using a regular grid, and the final spoiler was solid. For ease of reference, the term "porous" shall be used to collectively describe the effects of the regular grid and fractal grid spoilers.

Each spoiler had a width of $T_H = 247$ mm, a height of $T_V = 106$ mm, and a thickness of 4.76 mm (the imperial thickness of this is three-sixteenths of an inch, a standard industrial size). Spoilers 1–4, as well as the regular grid spoiler, had two 85×85 mm squares within them in which a fractal grid or regular grid was inserted. We use two different fractal grids with two different thickness ratios, $t_r = 3.02$ and 9. As well as varying the thickness ratio, the spacing between the two grids was also varied, with one set having the grids equally spaced along the spoiler (see Figs. 3a and 3c) and the other with an unequal spacing (see Figs. 3b and 3d) to determine the effect the frame size had, if any, on the noise. The blockage ratio σ for spoilers 1–4 in Fig. 3 was set to 75% due to the results from Sakaliyski et al. [10], who suggested that this blockage ratio would give the best acoustic performance.

The effective mesh size of the fractal grids, as defined by Hurst and Vassilicos [3], is shown in Eq. (2), where P is the perimeter of the shape and σ_g the blockage ratio of the grid (not σ, which is the blockage ratio of the spoiler listed in Table 1):

$$M_{\text{eff}} = \frac{4T^2}{P}\sqrt{1-\sigma_g} \tag{2}$$

This equation also applies to regular grids, in which case it gives $M_{\text{eff}} = M_g$, the mesh size of the regular grid, for which

$$\sigma_g = \frac{b}{M_g}\left(2 - \frac{b}{M_g}\right) \tag{3}$$

where b is the longitudinal thickness of the bars making the grid.

Two spoilers were also designed using a rectangular pattern (spoilers 5 and 6 in Fig. 3), which also had a thickness ratio of 3 and 9, however, the blockage ratio was decreased to 61%. Because this design incorporated a rectangular design, it meant that there would be two sets of dimensions for the lengths and thicknesses, while maintaining a constant thickness ratio for both the longer and shorter bars. For example, the size of the largest rectangle for the $t_r = 3$ and $t_r = 9$ are 59.23×146.22 mm and 63.29×156.24 mm, respectively, with corresponding thicknesses of 13.33×5.40 mm and 22.22×9.00 mm. A further spoiler was manufactured that had an equal spacing between the two grids, which were 116×116 mm in size, and had a t_r of 11. To achieve this, the blockage had to be reduced to 60%.

Table 1 gives a list of all the fractal spoilers used, along with their blockage ratios, thickness ratios, and spacings. It is important to note that the regular grid spoiler (see Fig. 3) has a similar design to spoilers 1–4 and as such has the same blockage ratio (i.e., 0.75). The spacing between the two grids is equal to the left and right frames, the bar thickness is 1.94 mm, and the mesh size is 7.55 mm, which is comparable to the effective mesh size of the fractal spoilers with the same blockage ratio. One can see from Eq. (3) that it is impossible to increase the mesh size without either decreasing σ_g or, if one wants to increase M_g while keeping σ_g constant, without increasing the bar thickness b on the grid. The latter would add to the low-frequency noise of the spoiler.

3. Possible Acoustic Sources of Fractal Spoilers

To understand how scaling the spoilers would affect acoustic performance, one must first have an idea of where the sources are located on the spoiler.

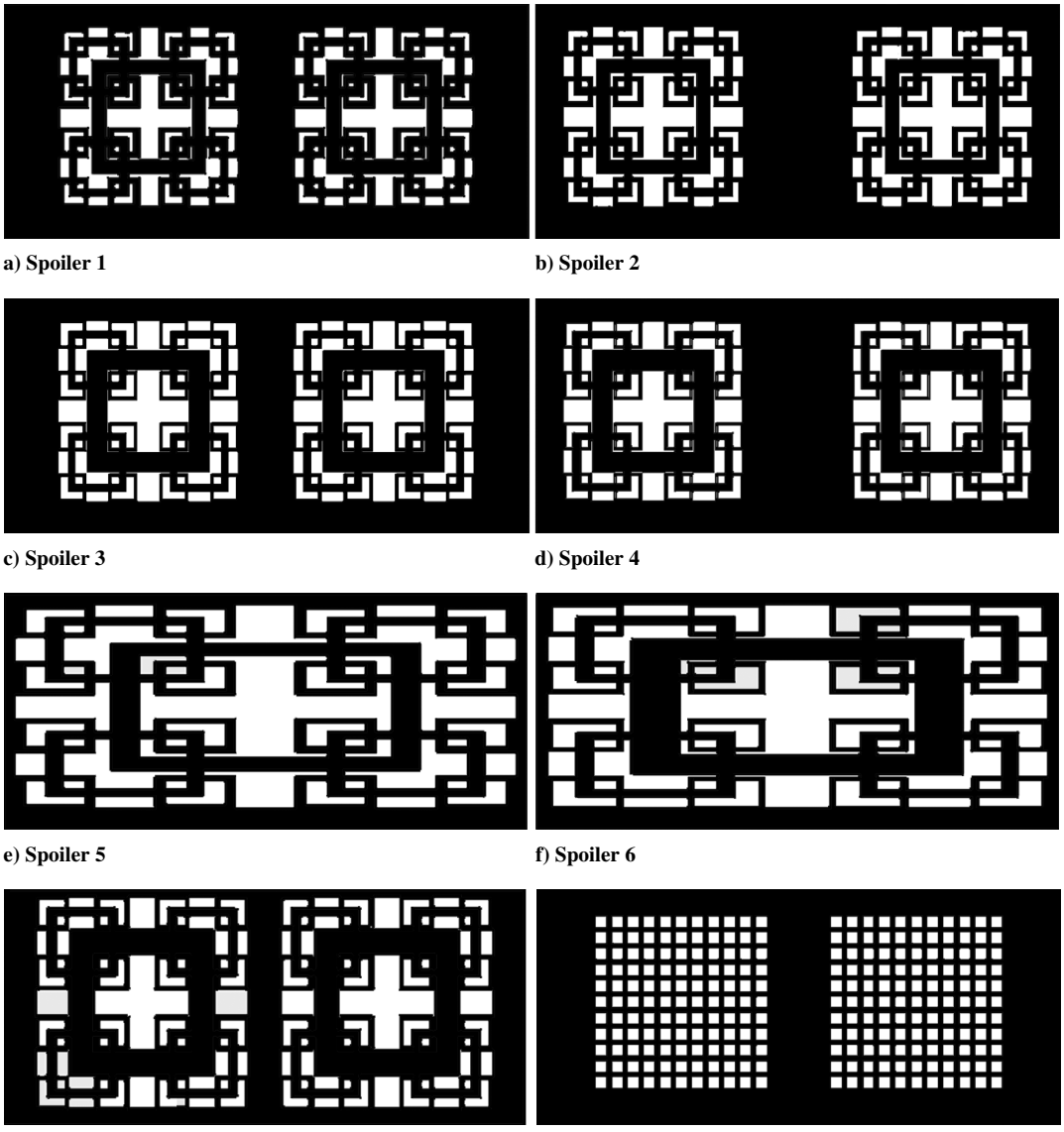

a) Spoiler 1 b) Spoiler 2

c) Spoiler 3 d) Spoiler 4

e) Spoiler 5 f) Spoiler 6

g) Spoiler 7 h) Regular grid spoiler

Fig. 3 Spoilers used during the experiments. Note lower frame is slightly thicker in all cases for mounting.

Sakaliyski et al. [10] showed that there are effectively three sources of noise on a porous spoiler: a bluff-body low-frequency noise due to the shedding off the top of the spoiler, a jet-like high-frequency noise from the holes, and the vibration of the spoiler itself. It is believed that the fractal spoilers would have similar sources in the shear layer shedding, however, the noise due to the spoiler vibration would be different and the noise due to the fractal porosity would be different to the jet noise produced by the holes. Concerning jet noise, fractals grids would have both jet-like noise sources and wake-like noise sources, due to the complicated interaction between the different elements of the fractal grid. The main jet source would be the central cross section, highlighted in gray in Fig. 4, whereas a

Table 1 Spoiler classification[a]

Spoiler	t_r	Spacing	Blockage ratio	l_0, mm	t_0, mm	R_L	R_t	M_{eff}, mm
1	3.02	Equal	0.75	47.45	5.95	0.5	0.58	7.32
2	3.02	Unequal	0.75	47.45	5.95	0.5	0.58	7.32
3	9	Equal	0.75	48.00	9.00	0.5	0.33	7.24
4	9	Unequal	0.75	48.00	9.00	0.5	0.33	7.24
5	3	Rectangular	0.61	——	——	——	——	——
6	9	Rectangular	0.61	——	——	——	——	——
7	11	Equal	0.60	57.14	11.00	0.5	0.30	——
Regular	1	Equal	0.75	7.55	1.94	1	1	7.55

[a]The ratio between the lateral thickness of the smallest and biggest bars is t_r; l_0 is the length of the biggest bar; t_0 is the lateral thickness of the biggest bar; R_L is the ratio of the successive bar lengths; and R_t is the ratio of successive bar thicknesses. The effective mesh size, obtained for the fractal grids using Eq. (2). The rectangular grid dimensions are not included because they are more complex and these grids are not comprehensively covered.

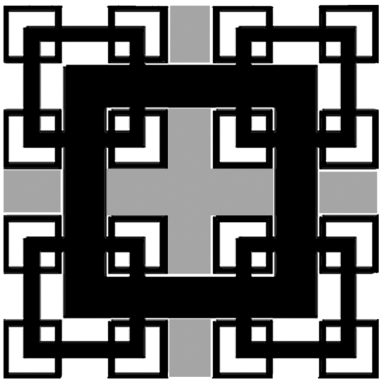

Fig. 4 Regions dominated by jet-like flow (gray) and wake-interaction flow (white) through a fractal grid.

wake-like flow may dominate in the square outside the cross, where the wakes from the different bars interact with each other, highlighted in white in Fig. 4.

According to Lighthill's acoustic analogy [25], the acoustic power of a jet would scale with the eighth power of the jet velocity, and since that initial study, extensive research has been carried out to fully understand the sources of jet noise. For comprehensive insight into jet noise developments since 1952, see Tam [12] and Karabasov [15]. Studies on jet noise have in the past considered a circular exhaust, however, in our fractal design, the jets are coming through a cross shape and would thus make it difficult to create an accurate velocity scaling law. A simple assumption that can be made is that the peak tonal frequencies associated with a jet would depend on the size of the orifice through which it flows, therefore, a smaller orifice, such as the circular holes in the plates by Sakaliyski et al. [10], would generate a higher frequency noise than the larger orifice seen in the fractal spoilers.

Curle [26] expanded Lighthill's acoustic analogy [25] to account for the case when an acoustic field interacts with a surface, using a circular cylinder as a practical example. He predicted that, at low speeds, where the von Kármán vortex street is observed, the sound is dominated by dipole noise sources and that the frequencies of the sound generated by the lift forces are equal to the shedding frequencies, whereas those generated by the drag force are twice the shedding frequency. This hypothesis was confirmed experimentally by Gerrard [27], where it was shown that the direction of this dipole is at right angles to the flow. Although we have rectangular cylinders in our fractal grids, Liow et al. [28] showed that the same mechanism is responsible for the acoustic sources for rectangular cylinders depending on their aspect ratio, namely, the shedding from the leading and trailing edge. The vortex shedding from the leading and trailing edge would therefore introduce two acoustic sources instead of the single source associated with a circular cylinder. Nevertheless, following Curle [26], one could use the Strouhal number to generate the expected frequencies due to each of the bars in the fractal grid; however, one must remember that there are several interacting wakes of varying length scales.

As well as the rectangular cylinders within the fractal grid, the frames around the edge of the fractal grids would also introduce wakes, which would mean that these would also be a source. Because of the larger size of the frames compared with the fractal dimensions, they are likely to create a lower frequency noise. It has already been mentioned, however, that the fractal spoiler has a combination of both multisized wakes and jets that interact with each other, including the jet-like flow coming through the two square holes.

III. Aeroacoustics of Inclined Wall-Mounted Spoilers

A. Experimental Setup

Acoustic and aerodynamic measurements of the wall-mounted spoilers were carried out at the University of Poitiers. Typically, spoilers are deployed over a range of angles between 8 and 30 deg. During landing, the spoiler is deployed at the highest angle, which has the biggest noise problem. We aim to explore the effectiveness of our spoilers at this extreme case. Therefore, the angle of 30 deg was chosen, however, a few acoustic tests were also done at 90 deg to demonstrate the effectiveness of the spoilers at higher angles.

The coordinate system is shown in Fig. 5. Aerodynamic force measurements of the inclined spoilers were made at Imperial College London. A range of velocities were used for the tests, ranging between 40 and 60 ms^{-1}. It has already been shown that the fractal grids have a variety of length scales, each of which could be used to define a different Reynolds number. For example, the Reynolds number based on the width of the spoilers T_H and a freestream velocity of 60 ms^{-1} would be roughly 9×10^5, which would be constant for all spoilers; however, if we were to choose the thickness of the largest bar, it becomes apparent that there are three possible Reynolds numbers: $Re_{t_0} \approx 38,000$ for spoilers 1 and 2, $Re_{t_0} \approx 57,000$ for spoilers 3 and 4, and finally $Re_{t_0} \approx 70,000$ for spoiler 7.

1. Acoustic Measurements

The acoustic measurements were taken in the Anechoic Wind Tunnel at the University of Poitiers. The wind tunnel has an acoustic range of 300 Hz to 16 kHz, is 2.8×3.8 m in size, and has a top speed of 60 ms^{-1}. For the purpose of these experiments, tests were run at 40, 45, and 50 ms^{-1}. The exhaust nozzle of the wind tunnel is 0.46×0.46 m and has a working section of length 1.3 m, with the collector having a cross section of 0.9 m in width and 0.9 m in height (see Fig. 5). A flat plate, of length 1.3 m, is placed between the opening and the collector, on which the mounting mechanism for the spoilers is located 0.5 m from the opening (see Fig. 5a). The background turbulence level of the flow is no more than 1% along the centerline of the tunnel.

Pressure measurements were obtained with a rack that had 16 Series 2, Bruel and Kjaer 4957 microphones arranged in a 4×4 grid, 0.15 m apart, calibrated using a 01 dB-Stell 9 V 6LR61 PP3-type 94 dB–1 kHz Pistonphone. During the experiments, the microphones were placed in two sets of locations, both of which were well outside the flow. For the top arrangement (Fig. 5b), the microphones were placed 1 m above the spoilers, measured from the surface, with the first line of microphones being in line with the leading edge of the

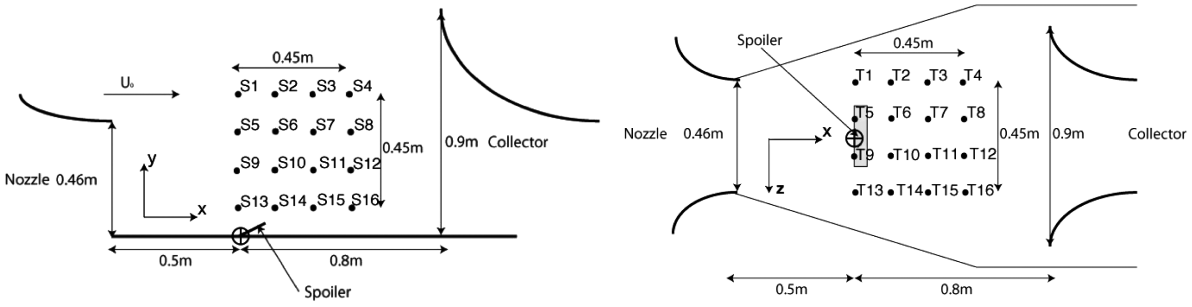

a) SIDE arrangement **b) TOP arrangement**

Fig. 5 Schematic of anechoic wind tunnel, showing location and numbering of microphones.

spoiler and along the centerline of the spoiler. For the side arrangement (Fig. 5a), the microphones were placed 1 m to the side of the spoiler, this distance being measured from the centerline of the spoiler, as well as 106 mm above the surface as seen in Fig. 5. Measurements were taken over a period of 20 s at a sampling frequency of 44 kHz. It is also worth noting that the numerical system used here for the microphones is for orientation purposes and that S4 and T4 do not mean that the same physical microphone was placed in these locations.

2. *Particle Image Velocimetry Measurements*

A particle image velocimetry (PIV) system has been used to record images of particles having a mean diameter 1 μm. The seeding is provided by a specially designed seeding grid located upstream of the convergent nozzle of the wind tunnel. The preprocessing corresponds to the subtraction of the background image using the minimum value within the set of images. Two-component velocity vector fields are computed with LaVision 7.2 software. A multipass algorithm with a final interrogation window size of 16×16 pixels and a 50% overlap is applied. The time interval separating the two laser shots was optimized to reduce out-of-plane errors while keeping the dynamic range for velocity measurements as large as possible. Spurious velocities are identified and replaced using both peak ratio and median filters.

One thousand statistically uncorrelated velocity fields were acquired with a LaVision Intense camera in a vertical plane along the centerline of the fractal square grids (note that this is not the same as the centerline of the spoiler) at a frequency rate of 4.5 Hz to generate converged turbulence statistics. This plane was chosen so as to capture the properties of the flow coming through the grids, as well as the shear layer created from the top of the spoiler. A second set of measurements were also taken in the *XZ* plane with the laser sheet located 4 mm above the surface, and it was the closest that we could get to the wall, where we were hoping to show the effect the spoilers had on the recirculation zone and ultimately on the low-frequency noise of the spoiler. The same plane also catches the shear layer formed by the edge of the spoiler, which, if combined with the PIV data from the *XY* plane, would give an adequate representation of the flow.

The resolution of the sensor is 1376×1040 pixels with a magnification size of 0.192 mm/pixel for the near wall planes. Illumination is provided by a double pulsed Nd:yttrium aluminum garnet laser emitting two pulses of 120 mJ each (laser sheet thickness ≤ 2 mm). The time interval between two laser shots is fixed at 10 μs for both PIV planes. The average percentage of spurious vectors removed with the postprocessing is approximately 0.5%.

3. *Force Measurements*

Measurements of the aerodynamic forces, acting on the spoilers, were carried out in the 0.46×0.46 m recirculating wind-tunnel at Imperial College London, which has a maximum speed of 60 ms^{-1} and a test section length of 1.5 m with the spoiler placed 0.5 m from the start of the test section. The freestream velocity was set at 40, 45, and 50 ms^{-1}, with the spoilers attached to two struts which were themselves attached to a Nutem Limited Force Balance (model number 528, serial number N336), which was capable of measuring lift and drag to an accuracy of ± 0.15 and ± 0.05 N, respectively. The spoilers were inclined by 30 deg and not attached to the wall, meaning the forces measured were acting on the spoiler alone.

It was found that the blockage of the experimental setup in the wind tunnel was 6%, which is low enough so that it does not require any blockage corrections. When obtaining the results for these experiments, there was a 2 min settle time to allow for any fluctuations.

B. Results

1. *Acoustics of Wall-Mounted Spoilers*

Acoustic measurements were taken for all the spoilers to determine which spoilers, if any, created the largest reduction in sound pressure level (SPL) [see Eq. (4)] compared with the solid spoiler:

$$\text{SPL} = 10 \log P_N \tag{4}$$

In Eq. (4), P_N is the spectral density of the nondimensional pressure ratio P/P_0, integrated over a bandwidth of 21 Hz, where P is the measured rms pressure and P_0 is the reference pressure set at 2×10^{-5} Pa. The importance of reducing the low-frequency noise has been mentioned several times, and to illustrate why this is the case, the narrowband spectra of the solid spoiler and spoiler 3 for microphone 4 in the top microphone arrangement (i.e., T4 in Fig. 5) is shown in Fig. 6. Note that the limits of the frequency have been set to $300 \leq f \leq 16,000$ Hz owing to the acoustic range of the wind tunnel in Poitiers. In this figure, the dominance of the low frequencies in the SPL of the solid spoiler can be clearly seen, which is why it is important to reduce the noise generated in this region. On the same graph, the narrowband spectra for spoiler 3 is also shown, where a SPL reduction is observed principally for the high level (low frequency), indicating a global reduction of the noise.

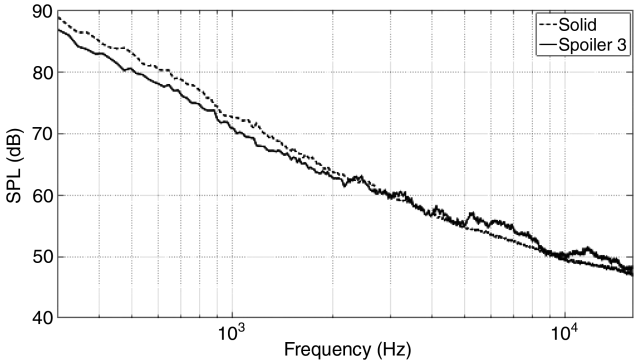

Fig. 6 Narrowband spectra for solid spoiler and spoiler 3, top microphone arrangement, T4 microphone, $U_\infty = 50$ ms^{-1}.

To illustrate the performance of the spoilers, the difference in SPL was obtained by subtracting the results of the solid spoiler from the chosen "test" spoiler (i.e., $\Delta\text{SPL} = \text{SPL}_{\text{Spoiler}} - \text{SPL}_{\text{Solid}}$), and so the graphs in Fig. 7 show how much noise the spoilers are making compared with the solid one.

Although pressure measurements were taken for all the microphones in the array, the results for the farthest microphone, based on the radial distance from the origin (see Fig. 5), are used because they are deemed to be indicative of the far-field radiation. For both top and side arrangements, microphone 4 would be the farthest, with a radial distance of 1.12 m for the top arrangement and 1.20 m for the side arrangement. After some initial analysis, it was found that the results from microphone 4 for the side arrangement gave results that were not consistent with the rest, and is therefore considered to be an outlier (see Fig. 8). As a result of this, the data from microphone 8 will be shown instead, which has a radial distance of 1.15 m.

The difference in SPL of all the spoilers is shown in Fig. 7, where we notice that, for the most part, the new spoilers generate less noise than the solid spoiler. For both cases, there seems to be a clear change where the fractal and regular grid spoilers suddenly begin to generate more noise, this change occurring at roughly 2 kHz. Despite this similarity, there is also a clear difference in spoiler performance between the two microphone arrangements. For the top arrangement (Fig. 7a), spoiler 3 shows the biggest reduction in the low-frequency range, roughly 2.5 dB, closely followed by spoiler 1, with spoiler 3 also showing the best performance in the higher frequencies. Both of these spoilers had the same spacing, however, spoiler 3 had a higher thickness ratio. Conversely, it is spoiler 4 that showed the worst performance, suggesting that the size of the central frame could be playing a role on the acoustic performance because the only difference between spoilers 3 and 4 is the size of the central frame and, therefore, the size of the edge frame. The exact opposite is seen

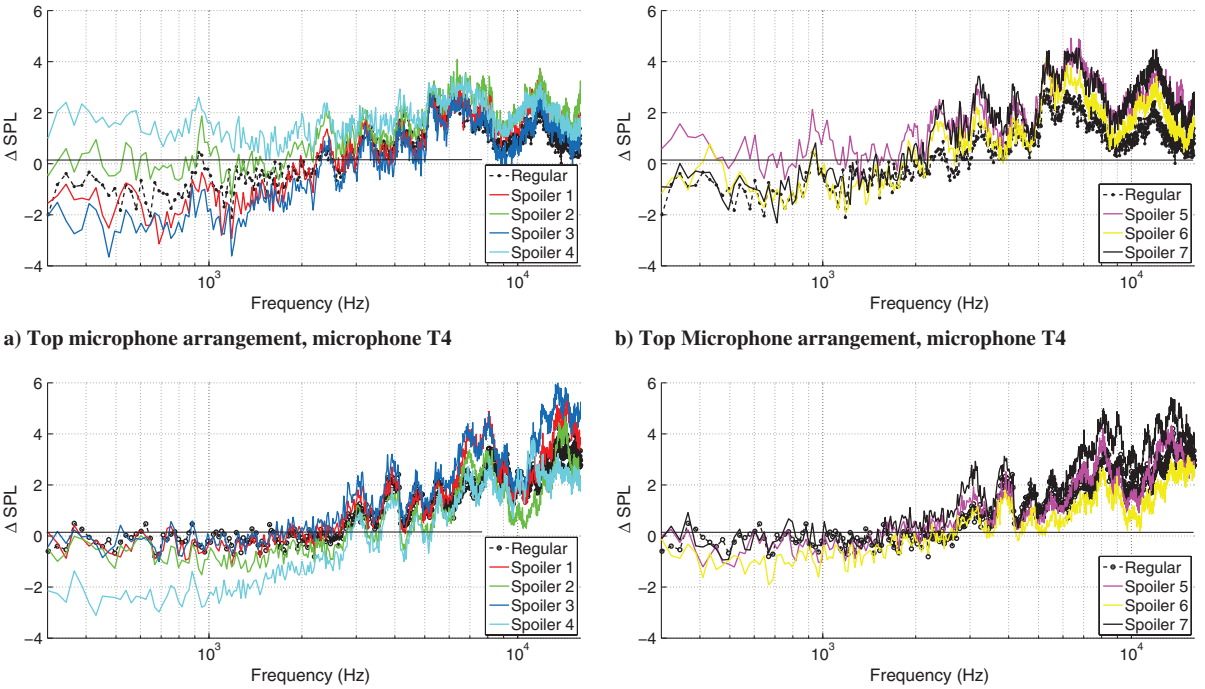

a) Top microphone arrangement, microphone T4

b) Top Microphone arrangement, microphone T4

c) Side microphone arrangement, microphone S8

d) Side microphone arrangement, microphone S8

Fig. 7 Far-field measurements showing the change in SPL between the spoilers and the solid spoiler, $U_\infty = 50$ ms^{-1}.

for the case when the microphones were placed to the side, in which case spoiler 4 showed the biggest decrease in SPL, and spoiler 3 was one of the worst.

To get a clearer view of their performance, the change in SPL for spoilers 3 and 4 compared with the solid spoiler are shown in Fig. 9. It has been shown that, for the top microphone arrangement, spoiler 3 seemed to be the best of our spoilers (see Fig. 7a), and using this spoiler as an example, the effects of increasing the thickness ratio and decreasing the central frame size are shown in Fig. 10. When comparing the SPL for spoiler 3 and spoiler 4, which is the same as seeing the effect of decreasing the central frame size (see Fig. 3), it is noticed that there is a 4 dB reduction in the SPL in the low-frequency range, and that this reduction decreases as the frequency increases. This suggests that the size of the central frame has a clear effect on the SPL radiating above the spoiler. The second line in Fig. 10 shows that the difference in SPL between spoiler 3 and spoiler 1 is roughly constant at 1 dB, suggesting that, by increasing the thickness ratio, a 1 dB reduction across all frequencies is observed. It is clear that increasing the t_r and decreasing the central frame size causes a reduction in the SPL.

The improvement in the SPL of the fractal spoilers is not limited to a single deflection angle of the spoiler, as can be seen in Fig. 11, where the spoilers are now deflected at an angle of 90 deg. Here we show the performance of spoilers 3 and 4 and the regular grid spoiler

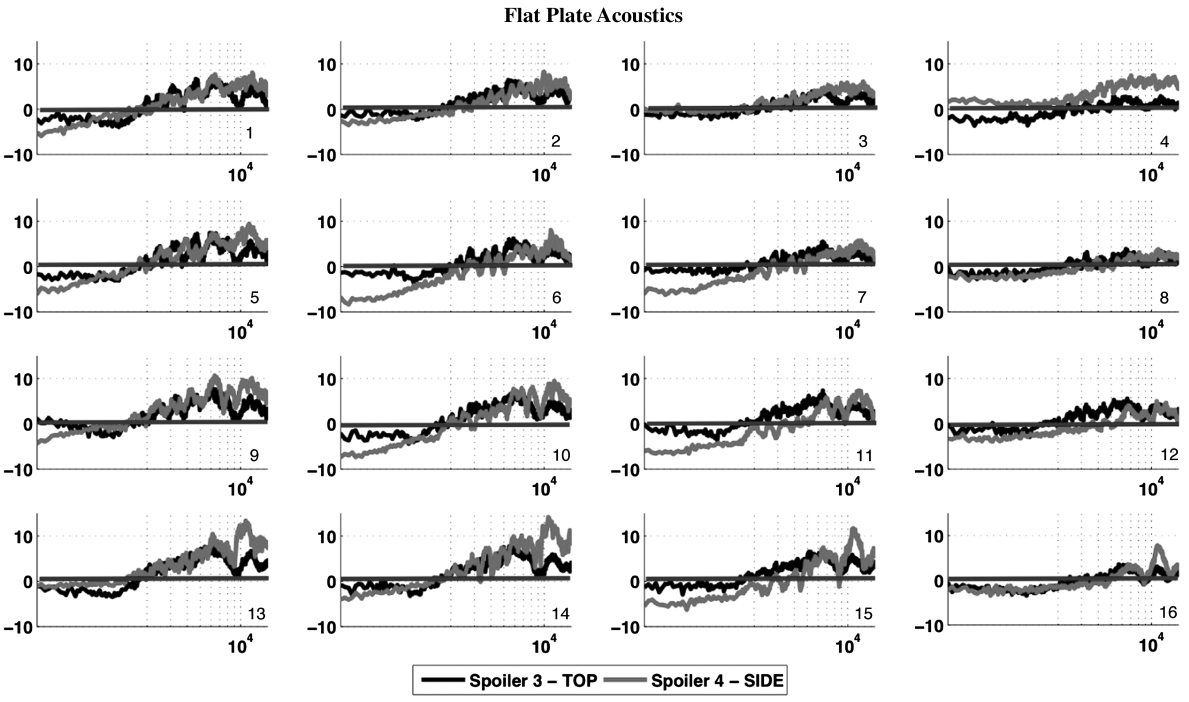

Fig. 8 Change in SPL for the two chosen spoilers at all microphone locations, $U_\infty = 50$ ms^{-1}.

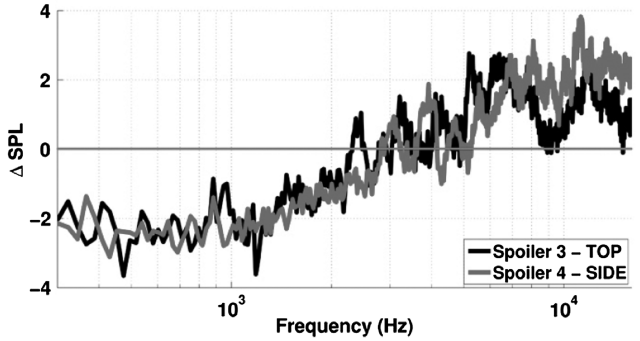

Fig. 9 Change in SPL of two chosen spoilers, $U_\infty = 50$ ms^{-1}.

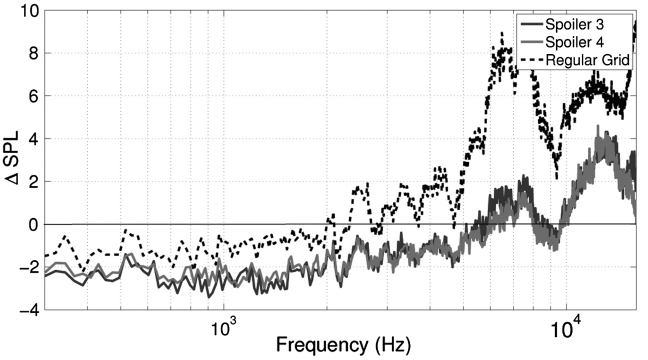

Fig. 11 Change in far-field SPL between the spoilers and the solid spoiler set at 90 deg. Microphone T4, $U_\infty = 50$ ms^{-1}.

compared with the solid spoiler, where it can be seen that the fractal spoilers have an improvement over a wider range of frequencies, especially in the higher frequencies. It is interesting that, at this angle, there appears to be no discernible difference between the two fractal spoilers.

2. *PIV Measurements of the Flow Behind the Wall-Mounted Spoilers*

Two PIV planes were used to study the flow behind the spoilers. The first of these was in the XY plane, in line with the center of the fractal grids, the results of which can be seen in Fig. 12. Along with the normalized U-mean velocity, the spanwise mean vorticity as well as the streamwise and wall-normal turbulence intensities are shown. A striking conclusion that can be made from these results is that the top frame of the spoilers is dominating a large region of the flow behind it. In particular, the wake generated by the top frame attributes to roughly 50% of the flow behind the spoiler, as seen in the streamwise mean velocity plots in Figs. 12b and 12c. The recirculation region generated by this wake is bigger for the regular grid spoiler than it is for the fractal spoiler, something which could affect the frequency and the intensity of the noise produced by the spoilers. These results also show that there is no recirculating bubble attached to the spoiler and the wall, as is seen in Fig. 12a, which indicates that the main bubble has become detached from the spoiler.

The associated spanwise mean flow vorticity for the shear layer coming from the top of the spoiler and the wake of the top frame is seen in Figs. 12e and 12f, but what is interesting is the increased level of vorticity immediately behind the fractal grids, suggesting an increased level of turbulent mixing over a wider region compared with the regular spoiler. Increased levels of both u and v turbulence intensity is seen for the fractal spoiler, suggesting that the flow coming through the spoiler is more turbulent than the regular grid. These results coincide with our original assumption that the bleed air of the fractal spoiler has more mean vorticity, velocity, and turbulence intensity than the regular grid spoiler. What cannot be seen from these PIV results, however, is wether or not the "bubble" has been removed entirely, or if it has simply moved further downstream. For this, the XZ plane must be studied.

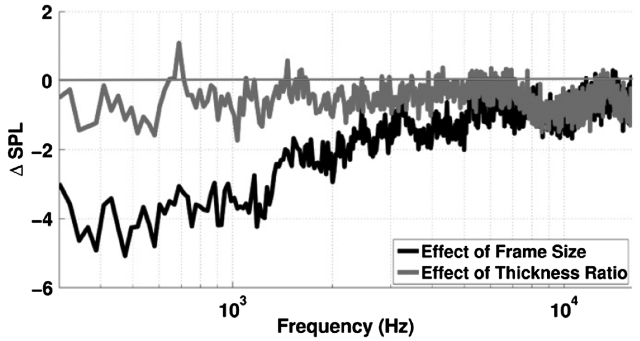

Fig. 10 Effect of decreasing frame size ($\mathrm{SPL}_{\mathrm{Spoiler3}} - \mathrm{SPL}_{\mathrm{Spoiler4}}$) and increasing thickness ratio ($\mathrm{SPL}_{\mathrm{Spoiler3}} - \mathrm{SPL}_{\mathrm{Spoiler1}}$). $U_\infty = 50$ ms^{-1}.

Figure 13 shows the U-mean velocity and the 2-D turbulent kinetic energy (TKE) for the solid spoiler, regular grid spoiler, as well as spoilers 3 and 4 in the XZ plane located 4 mm from the surface. The U-mean velocity for the solid spoiler (Fig. 13a) shows that the recirculating region extends to three chord lengths downstream (i.e., up to $x \approx 3T_V$), however, the wake of the spoiler continues beyond $x \approx 4.5T_V$. For the regular grid spoiler, the recirculating region, defined as the area of negative mean velocity, is found between $x \approx 2.5T_V$ and $x \approx 4T_V$ and it is also found for spoiler 4, where it appears to have the same size, but is closer to the spoiler. Interestingly, there does not appear to be any region of recirculating flow for spoiler 3 because all the values in Fig. 13e are positive with the mean velocity decreasing to just above zero. This is also seen in Fig. 14, where the velocity along the centerline of the spoiler ($z = 0$) decreases as we move further downstream before beginning to increase again at around $x \approx 4T_V$ for spoiler 3. The results suggest that there is a region of very slow or possibly stagnant flow behind spoiler 3 and that the size of the central frame has a clear impact on the flow being generated behind the spoiler. Furthermore, the effect of the fractal grid can be seen when comparing the results of the regular grid spoiler and spoiler 3 because both have the same central frame size, where we note that, with the fractal grid, the recirculation region is no longer present.

The turbulent kinetic energy of the flow in the XZ plane gives a good indication of the sound-generating mechanisms because we are very close to the surface ($y = 4$ mm). The results for the solid spoiler show a large amount of TKE compared with the other spoilers immediately behind the recirculating region. In comparison to the solid spoiler, the three porous spoilers (Figs. 13d, 13f, and 13h) show reduced levels of TKE behind the spoiler with the shear layer from the side of the spoilers generating the highest levels of TKE. Of these, it is the regular grid spoiler that is showing higher levels of TKE in the shear layer than the two fractal spoilers. Not only that, but there is a clear region between $x \approx 2T_V$ and $x \approx 2.5T_V$ where there is a slight increase in TKE, which corresponds to the region where the jet flow through the grid meets the recirculating region. A similar area can be seen for spoiler 4 in Fig. 13h, where the region of increased TKE close to the spoiler corresponds to the boundary between jet flow and the recirculation region. For completeness, the TKE along the centerline is shown in Fig. 14.

3. *Aerodynamic Force Measurements*

As mentioned in the experimental setup section, the force measurements were just of the spoiler, not mounted on the wall. The results presented here are more to show how the lift and drag being exerted on the spoiler vary as the fractal parameters are changed and are of no direct relevance to the wing-mounted spoiler configuration that we discuss in Sec. III.

Although the coefficients of lift and drag are useful when it comes to scaling, they can be misleading when one wants to compare the performance of two devices. Any new spoiler should not change the amount of lift and drag being exerted on it because they are designed to reduce a certain amount of lift and increase a certain amount of drag during flight conditions. Therefore, the percentage change in lift

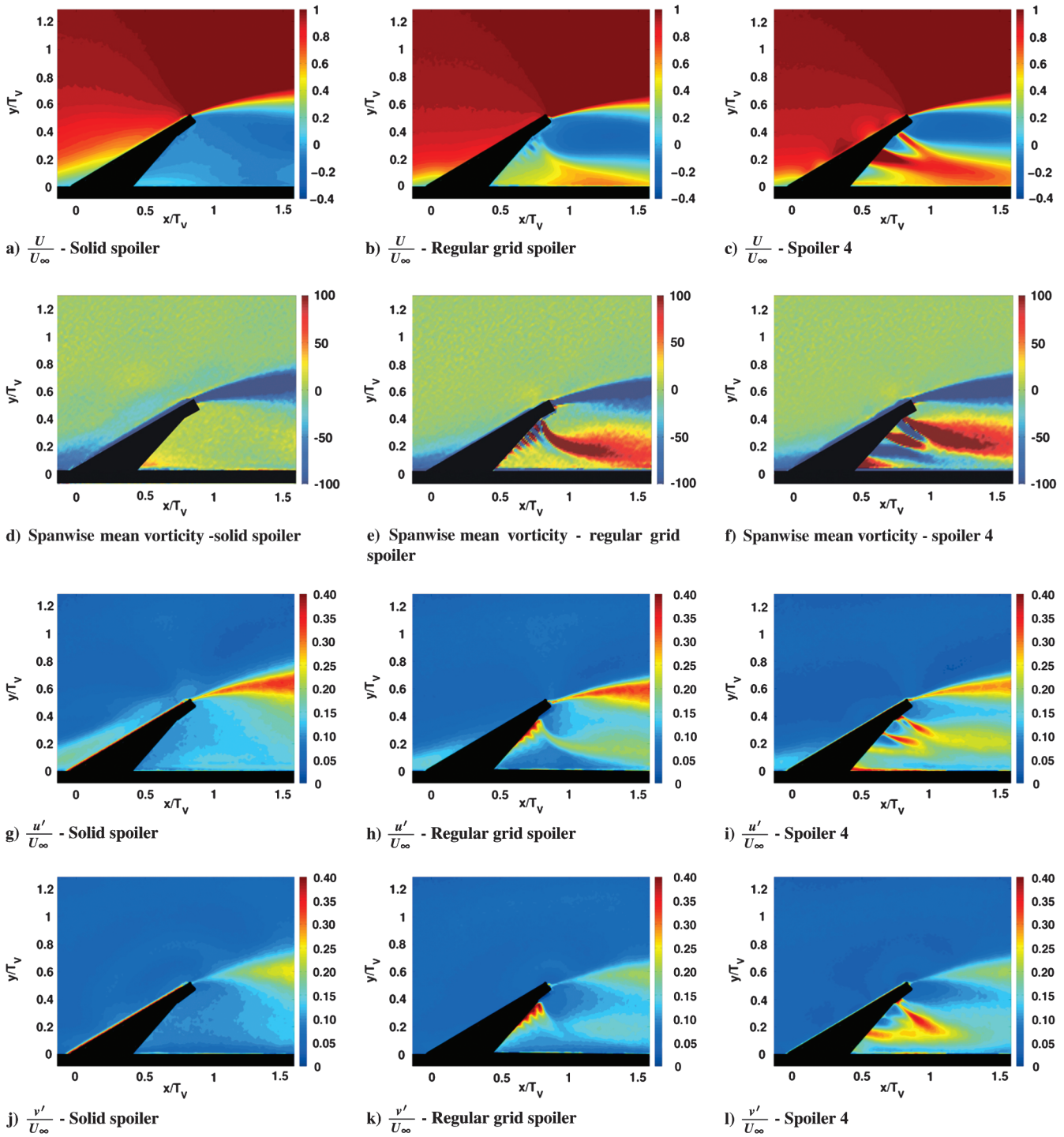

Fig. 12 *XY* **plane PIV results for solid spoiler, regular grid spoiler, and spoiler 4 at $U_\infty = 40$ ms^{-1}.**

and drag force compared with the solid spoiler, P_L and P_D, are shown in Table 2, in which a negative value indicates a percentage decrease in the lift force compared with the solid spoiler.

The first conclusion to be made from these results is that the lift force acting on the spoiler decreases when porosity is introduced, however, all except one of our spoilers are able to generate more drag, with the regular grid spoiler having almost 10% more drag force than the solid spoiler. There also appears to be a distinct influence of both thickness ratio and frame size on the forces being exerted on the spoiler; for example, if the results for spoilers 1–4 are looked at further, one would notice that, by increasing thickness ratio (i.e., comparing spoilers 1 and 3 and similarly spoilers 2 and 4), there is a clear increase in drag force and a reduction in lift. If the results from spoilers 3 and 4 are compared, then a reduction in drag and an increase in lift is seen, suggesting that the size of the frame as well as the thickness ratio influence the aerodynamic forces being exerted on the spoilers.

The increase in drag is also seen in the coefficient of drag, where it is seen that C_D for all the spoilers is greater than the solid spoiler. Similarly, the coefficient of lift for the spoilers are all less than the solid spoiler, with some closer than others, where the total area of the spoiler ($T_V \times T_H$) is used to calculate both the coefficients of lift and drag. Note also, though, that the regular grid spoiler's decrease in lift relative to the solid spoiler is nearly double its decrease in blockage ratio, whereas this decrease is between roughly 1 and 1.5 the decrease in σ for spoilers 1–4. Also, the ratio of lift to drag hovers around 1 for these four spoilers, whereas it is only 0.8 for the regular grid spoiler.

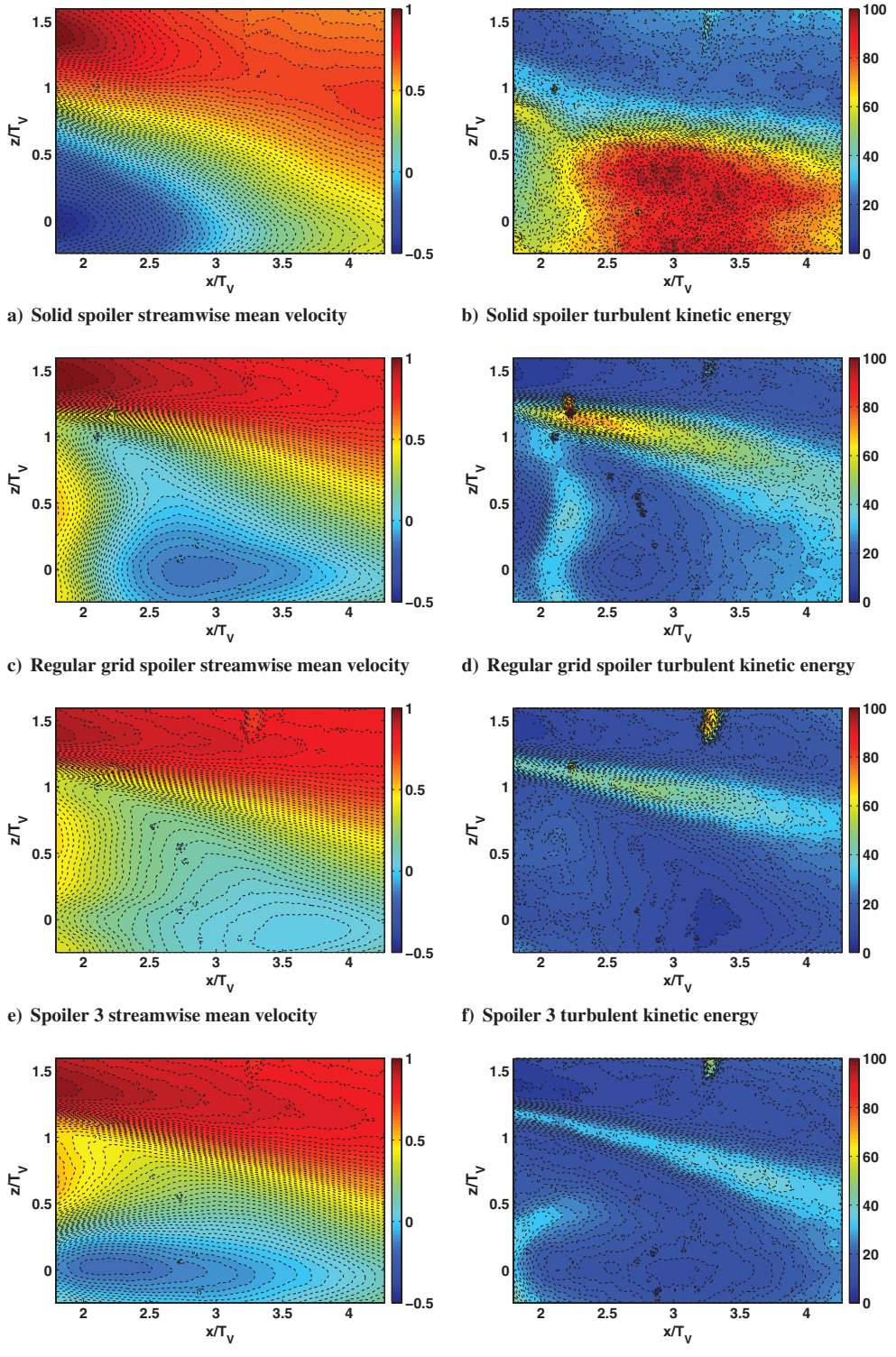

a) Solid spoiler streamwise mean velocity

b) Solid spoiler turbulent kinetic energy

c) Regular grid spoiler streamwise mean velocity

d) Regular grid spoiler turbulent kinetic energy

e) Spoiler 3 streamwise mean velocity

f) Spoiler 3 turbulent kinetic energy

g) Spoiler 4 streamwise mean velocity

h) Spoiler 4 turbulent kinetic energy

Fig. 13 *XZ* plane PIV results for solid spoiler, regular grid spoiler, and spoilers 3 and 4, 4 mm from the surface, $U_\infty = 40$ ms^{-1}.

Again, just as was seen for the acoustic results, by varying the thickness ratio and the size of the frame, different results can be achieved for the lift and drag forces.

C. Discussion

The results for the wall-mounted spoilers have shown clears signs that thickness ratio and frame size play a key role on the aerodynamics and acoustics around the spoilers, however, a lot of questions still remain unanswered. How would these spoilers perform if they were scaled up? How can we scale these spoilers and, probably most importantly, how can the design of these spoilers be improved upon?

1. *Spoiler Scaling Methods*

The reduction in SPL, both on the flat plate and on the real wing section, does suggest the possibility of using fractal spoilers to reduce the noise. Despite the relatively small scale of the model, it was still possible to show design effects on the aeroacoustic performance by making very small changes, as can be seen in Fig. 3, with these small variations showing clear differences in the results. The main

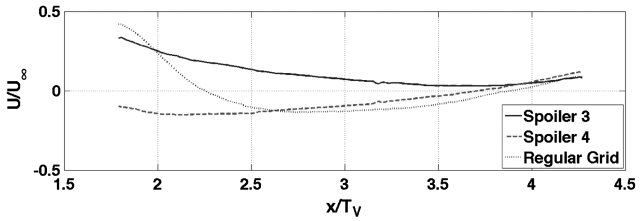

a) Normalized streamwise velocity

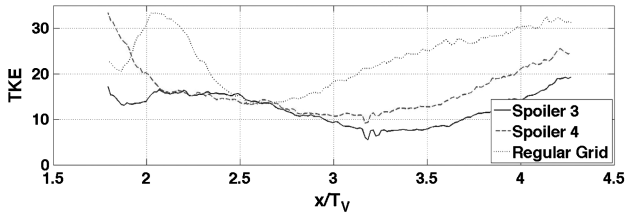

b) Turbulent kinetic energy

Fig. 14 Normalized streamwise velocity and turbulent kinetic energy along the centerline 4 mm from the surface, $U_\infty = 40$ ms^{-1}.

constraint in designing the fractal grids came as a result of machining constraints as well as the mathematical nature of fractals; the smallest thickness of the bars that make up our fractal spoilers was set to 1 mm because this was the limit of the machines. This, and the overall size of the fractal spoiler, meant that there were certain limitations to the fractal parameters as well, such as a maximum thickness ratio t_r. If, for example, we were to use a model that was twice the size of what we currently have (i.e., if the spoiler would have a height and width of 212 and 494 mm, with internal squares being 170 × 170 mm, with the same machining constraints and blockage ratio), the maximum possible thickness ratio would be 21. This is not to say that we have to use this value, but merely shows the increased range and flexibility one would get by only slightly increasing the size of the spoiler.

The scaling of the fractal spoilers can be done in two different ways. First, a direct scaling of all the parameters, while keeping the number of fractal iterations the same, would mean an increase in the minimum thickness and hence an increase in the turbulent length scales introduced. Using this method, however, will mean that the thickness ratio remains constant, as well as the number of fractal iterations. Alternatively, if we are to believe that by introducing the smaller length scales we can change the acoustic signature over a wide range of frequencies, then it would be beneficial to have as many of these smaller length scales as possible in the design and therefore increase the number of fractal iterations as we scale up.

We now briefly present data from the side microphone arrangement for spoilers 3 and 4 for all three velocities, $U_\infty = 40$, 45, and 50 ms^{-1}, where a fourth power of the Mach number scaling

Table 2 Aerodynamic values of spoilers obtained from the force balance[a]

Spoiler	P_L, %	P_D, %	C_L	C_D	L/D	P_σ, %
Solid	27.42 N	16.80 N	0.65	0.40	1.63	0.026 m^2
Regular	−46.00	10.56	0.35	0.44	0.80	−25
1	−29.46	6.91	0.46	0.43	1.08	−25
2	−34.71	6.84	0.43	0.43	1.00	−25
3	−32.15	9.68	0.44	0.44	1.01	−25
4	−39.76	7.87	0.39	0.43	0.91	−25
5	−67.35	0.42	0.21	0.40	0.53	−39
6	−69.54	−4.84	0.20	0.38	0.52	−39
7	−48.00	3.15	0.34	0.41	0.82	−40

[a]P_L and P_D are the percentage change in the lift and drag forces at $U_\infty = 50$ ms^{-1}, respectively, compared with the solid spoiler (a negative value indicating a percentage decrease). For the solid spoiler, forces acting on it are shown. P_σ is the percentage change in blockage ratio compared with the solid spoiler. The area used for the coefficients is defined as $T_V \times T_H$.

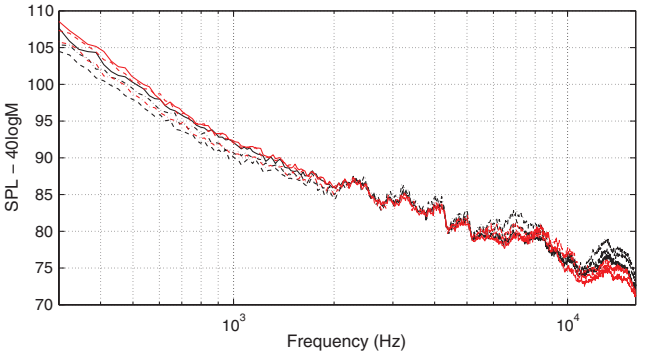

Fig. 15 Velocity scaling for spoiler 3 (black) and spoiler 4 (red) for the side microphone arrangement.

has been applied, as can be seen in Fig. 15. Here, we can see that this is a good fit for both spoilers, but only in a specific range of frequencies: $2000 \leq f(\text{Hz}) \leq 6000$. A similar fit was successfully implemented by Sakaliyski et al. [10], who also found that a high-frequency M^4 scaling worked well with their data. They explained this result in terms of a uniform and regular array of jets from their plates.

2. *Factors Affecting the Sound Pressure Level and Design Optimization*

Spoilers 1–4, as well as the regular grid spoiler, all have the same upper frame size with the results from the top microphone arrangement suggesting that a larger thickness ratio and smaller central frame will result in an improved performance. For the side microphone arrangement, we again see that it was the spoiler with the highest thickness ratio and smaller side frame size that gave the best acoustic performance. This suggests that a spoiler with a high thickness ratio and a small frame size at the side and top should give the best results in both directions.

The effect of frame size on the flow behind the spoiler can be seen in the PIV results, particularly in the XZ plane, with spoiler 3 showing no signs of a recirculation region or increased levels of turbulence kinetic energy downstream of the spoiler (Figs. 13e and 13f). Compare this with spoiler 4, where, by increasing the central frame size, a recirculation region and the associated TKE appear behind the spoiler, and then we begin to see why spoiler 3 shows a bigger SPL reduction for the top microphone arrangement. These observations, however, are based on mean-velocity vector fields and it is entirely possible that the recirculation region exists for spoiler 3 when instantaneous images are considered, as seen in Fig. 16a. An instantaneous u-velocity vector field for the regular grid spoiler, spoiler 3, and spoiler 4 are shown in Fig. 16, where the white region in the figures represents the region of recirculating flow, thus making the bubble easier to see. Evidently, instantaneous reverse flow does exist for spoiler 3, suggesting it must appear and then disappear because the mean-velocity vector field shows no sign of recirculating flow. It can also be noted that the size of the bubble is larger for spoiler 4 than it is for spoiler 3, however, to be able to relate this to the acoustics of the two spoilers, one must know how this region fluctuates.

To determine the fluctuations of the recirculation region, the area of the bubble for each instantaneous image was found. To combat the influence of possible bad vectors that appear in the region $z/T_V > 0.8$ due to the tape on the wall coming lose during the experiment (note that these experiments were not done at the same time as the acoustic measurements), we only consider the flow in the region $0 \leq z/T_V \leq 0.8$ and use that area to normalize the area of the recirculation region. A probability density function (PDF) of the normalized bubble area σ_B is shown in Fig. 17a, where the regular grid spoiler is showing a wider spread, suggesting larger fluctuations of the recirculation region. What is interesting from Fig. 17a is that spoilers 2 and 4 seem to have almost identical PDFs, suggesting that, with the fractal grids further apart, increasing the thickness ratio has no effect on the recirculation region. This is confirmed in Fig. 17b, where the PDF of

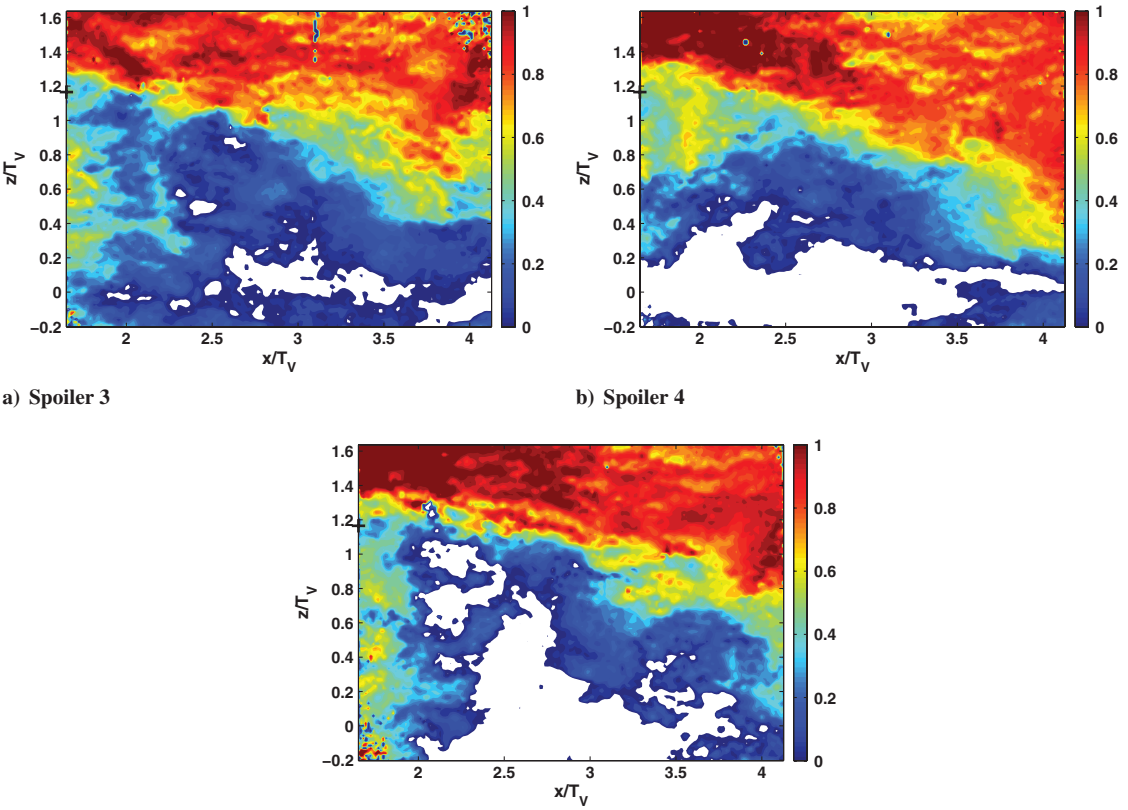

a) Spoiler 3 b) Spoiler 4

c) Regular grid spoiler

Fig. 16 Instantaneous u-velocity vector field for three spoilers. Edge of spoiler located at $z/T_V = 1.16$, $U_\infty = 40$ ms^{-1}.

the mean length of the bubble, taken in the same domain as the area, is shown and we again see that spoilers 2 and 4 have almost identical PDFs.

Unlike spoilers 2 and 4, spoilers 1 and 3, which have the two fractal grids closer to each other (Fig. 3), increasing the thickness ratio shifts the PDF toward zero, with spoiler 3 showing, as was suspected, that the recirculation region fluctuates between existing and not existing. Knowing that the bubble has a small area and that the fluctuations are small would explain why spoiler 3 is showing the biggest reduction in SPL for the top microphone arrangement. Combining these results, it can also be argued that, because the most probable mean length of the bubble for the regular grid spoiler is less than that of spoilers 2 and 4, yet the area of the bubble for all three are similar, the bubble for the regular grid spoiler must be wider than the ones from spoilers 2 and 4. A similar argument can be used for spoilers 1 and 3, as can be seen in the instantaneous PIV results in Fig. 16.

These PIV results could also explain why there are differences between the measurements from the top and side microphone arrangement. By decreasing the size of the side frame size and increasing the turbulence intensity of the bleed flow, it is believed that the recirculation region of the side frame would reduce in size and along with it the intensity of the shear layer. This can be seen in Figs. 13f and 13h, where the TKE of the shear layer is lower for spoiler 4, which has the smaller side frame, than it is for spoiler 3, although it is important to remember that this PIV plane is two chord lengths downstream. It is also possible that the presence of a recirculation region would inhibit the fluctuation of the side shear layer and thus possibly decrease the low-frequency noise radiated to the sides, which could explain why spoiler 3 is producing more low-frequency noise to the side because there is no recirculation region to inhibit the fluctuation. This would have to be studied in more detail to fully understand the mechanisms involved.

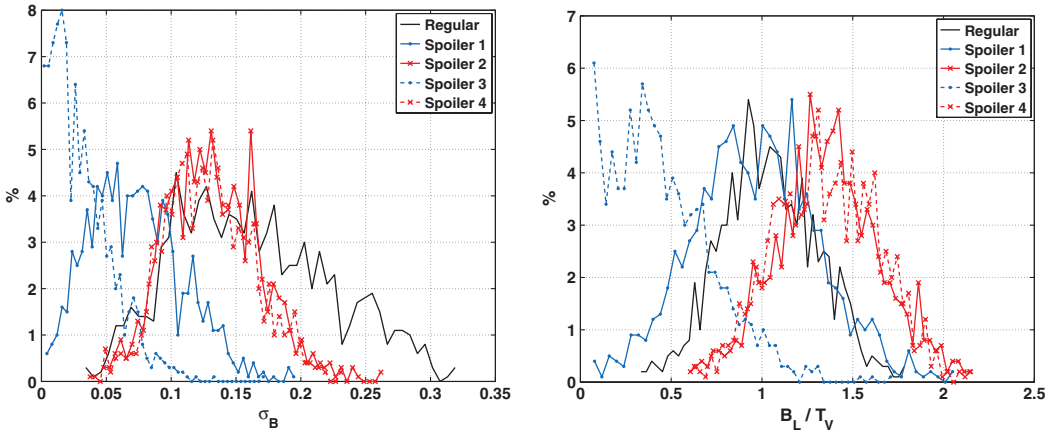

a) Normalized bubble area b) Mean bubble length

Fig. 17 PDF for the normalized bubble area, σ_B, and the mean length of the recirculation region, $U_\infty = 40$ ms^{-1}.

What the results do suggest is that the ideal spoiler would be one with a high thickness ratio and as small a frame as possible with the two fractal squares as close to each other as possible. However, this does not seem to be the case because spoiler 7, which had both of these as well as a decrease in blockage ratio, performed worse than spoilers 1–4. Similarly, spoilers 5 and 6, which had a rectangular fractal design as well as smaller frame sizes, also performed worse than spoilers 1–4.

Going back to the original ideas on fractal spoilers, it seems a little counterintuitive that, by decreasing the blockage ratio, the acoustic performance is worse because, by letting more bleed air through with a high-turbulence intensity, the recirculation region should be removed entirely. It appears that there is also an optimum blockage ratio for the best acoustic performance, which appears to be, just as Sakaliyski et al. [10] found in their study, around 75%. One possible reason for this is as follows: By decreasing the blockage ratio, the spoiler lets through more bleed air and so the momentum passing through the spoilers and onto the surface is increased. This increase of fluctuating momentum and turbulence kinetic energy on the surface, seen for spoilers 5 and 6 in Figs. 18a and 18b, would be detrimental to the acoustic signature of the spoiler. Note that the scale of these two figures is the same as the ones in Fig. 13 and that the effect of increasing the thickness ratio (see Table 1) is clearly seen, with spoiler 6 having higher levels compared with spoiler 5, which have thickness ratios of 3 and 9, respectively. Again, what is not visible is the region close to the spoiler where the majority of the bleed air would be impacting on the surface. This problem would not exist on the wing section because, when a spoiler is deployed, there is an opening and so the flow would not impact on any surface, which could mean that, on the wing section, spoiler 7 might perform better than spoiler 3.

A simplified argument of these results would be this: If you have two spoilers, identical in both size and blockage ratio and subjected to the same freestream conditions, however, one has a fractal design and the other uses a simple porous design, both would have less noise than the solid spoiler, but with the fractal spoiler having even less than the porous one. Both the porous and fractal spoilers will introduce bleed air that will force the recirculation region to become detached from the spoiler and move downstream. However, due to the increased levels of turbulence intensity, as well as the increased velocity through the spoiler (Fig. 12c) (i.e., an increased amount of momentum compared with the porous spoiler), the fractal spoiler is able to reduce the size of the bubble more than the porous one. It is therefore more appropriate to think in terms of the momentum and intensity of the bleed air coming through the spoiler and decouple this with the blockage ratio argument put forward by Castro [20]. Instead, the question should be, how intense should the bleed air be to remove the recirculation region without making the openings in the spoiler too big that they themselves introduce a low-frequency noise?

It is believed that the ideal design of such a spoiler would have small openings and thicknesses so that the noise generated by its own shape will be in the high-frequency range and not contribute to the low range, which is what we are trying to remove in the first place, yet at the same time, create a high-momentum bleed flow to remove the bubble. Using fractals, this can be achieved and, by scaling up the design, there is the added freedom to increase the turbulence intensity and momentum, without changing the blockage. The fractal grids currently use rectangular shapes to generate the turbulent flow behind it; however, if circular shapes were used, it is believed that the SPL would be reduced further. King and Pfizenmaier [29] showed that, for a single cylinder subjected to a freestream, a cylinder with a circular cross section would generate up to 10 dB less noise than a cylinder with a square cross section. Naturally, if the spoiler had rounded edges, one would expect an improved acoustic performance than is seen with the current design.

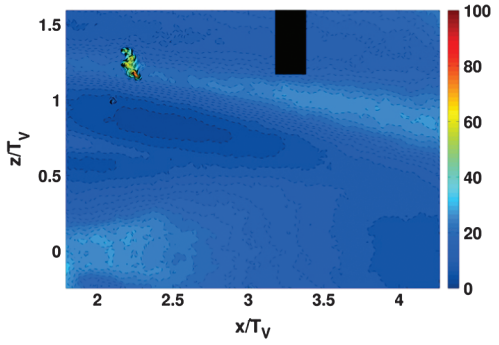

a) Spoiler 5

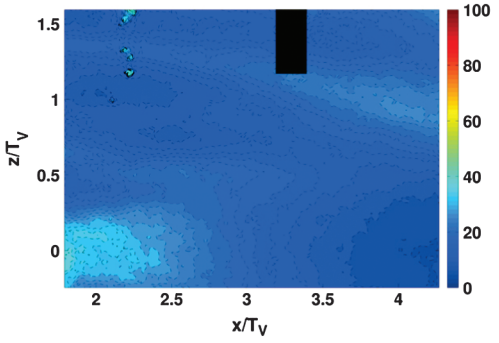

b) Spoiler 6

Fig. 18 Turbulent kinetic energy $[\frac{1}{2}(u'^2 + w'^2)]$ in the XZ plane, 4 mm from the surface, $U_\infty = 40$ ms^{-1}. Black area are invalid vectors.

IV. Aeroacoustics of Wing-Mounted Inclined Spoilers

A. Experimental Setup

Combined aeroacoustic measurements were carried out in the Acoustic Wind Tunnel Brunswick (AWB) at the DLR Institute for Aerodynamics and Flow Technology, Germany. AWB is a low-noise closed-circuit tunnel with an open test section in an anechoic test hall of dimensions $6.9 \times 6.9 \times 3.51$ m. The nozzle has a cross section of 1.2×0.8 m and a maximum wind speed of 65 ms^{-1}, however, for the purpose of these tests, the wind-tunnel speed was set at 40, 50, and 60 ms^{-1}, where the background turbulence level is 0.3% at a freestream velocity of 60 ms^{-1}. A feature of the AWB is the adjustable collector, which is located 3.65 m from the nozzle and can move in the streamwise and vertical direction, thus enabling it to capture the flow from experiments involving high angles of attack. For these tests, the collector was shifted 60 mm downward.

A three-element high-lift wing system is placed in front of the nozzle, which is capable of having various angles of attack α, as seen in Fig. 19. The main wing section has a chord length of 0.3 m and a span of 0.8 m, and is based on the wing of the A320. At the front of the wing section, there is a leading-edge slat that is deflected at 25 deg, whereas, at the trailing edge, there is a flap that is deflected at 30 deg.

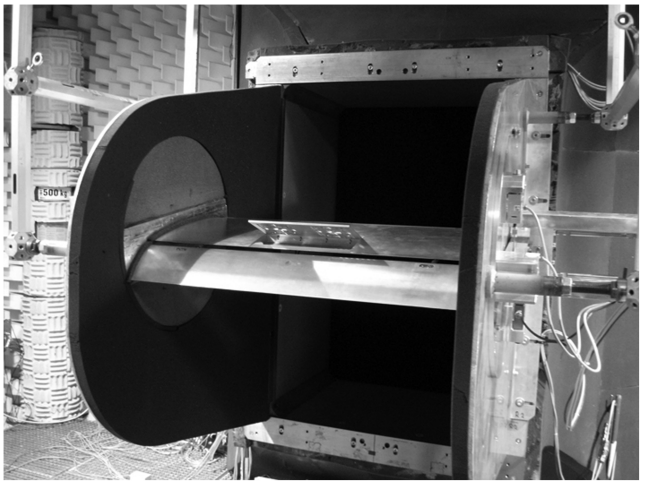

Fig. 19 Wing mounted spoiler set-up in AWB.

Three angles of attack were chosen: 9, 12, and 15 deg, with the spoiler deflection set at 30 deg.

Below the wing system, seven Bruel and Kjaer 4134 microphones were placed outside the flow, spanning a range of polar angles between $63 \leq \phi \leq 124$ deg; the fourth microphone is placed directly below the spoiler and has a polar angle ϕ of 90 deg from the direction of the freestream flow. The entire wing system is connected to a force balance to obtain pitch, lift, and drag forces. Data were collected at a sample frequency of 115 kHz and a sample time of 26 s for each angle of attack and each velocity, giving a 28 Hz bandwidth of integration for the SPL.

B. Results

1. *Acoustic Performance of Fractal Spoilers*

For these tests, only two spoilers could be investigated and, based on the experiments described in Sec. II, spoilers 3 and 4 were selected. Just as it was in our previous experiments, the acoustic performance of the two spoilers is based on the difference in SPL to the conventional (solid) spoiler; a negative difference indicating a decrease in SPL. Figure 20 shows both the narrowband spectra for the solid spoiler and fractal spoilers, as well as the change in SPL caused by the fractal spoilers for the overhead ($\phi = 90$ deg) radiation.

The first thing to note from this figure is that, for all spoilers, there is very little difference in the acoustic signal for all angles of attack, and the second thing to note is that two very distinct tonal peaks exist at 1.7 and 2.5 kHz. These two tonal frequencies are in fact due to the slats and associated cavities from the three-element wing system and are not associated with the spoiler; they are also found to diminish with increasing angle of attack. There also appears to be little difference in the SPL between the two fractal spoilers.

From the second figure, we see that the presence of the fractal spoilers create a reduction in the low-frequency noise for the entire wing system, with a reduction of up to 4 dB seen below 2 kHz. Even in the higher frequencies, a small reduction is seen between 0.5 and 1 dB up to frequencies of roughly 6 kHz, whereas, as we reach the limit of the human hearing range, they cause an increase of up to 1 dB. There are also signs that, for the very low-frequency range (≤ 500 Hz), by increasing the angle of attack, the reduction in SPL begins to diminish, however, the difference is quite small.

2. *Aerodynamic Performance of Fractal Spoilers*

If the spoiler is to be considered as a replacement for the current spoilers seen on aircraft, it is imperative that the lift and drag characteristics of the wing system remain unchanged, therefore, as with the previous tests, it is the percentage change in the lift and drag force that are the ultimate criteria when it comes to comparing the spoilers to the conventional arrangement. From Table 3, it can be seen that there is very little change in the lift forces acting on the entire wing system across all wing angles of attack, with the percentage change varying from −0.53% to 1.36%. The percentage change in drag force is slightly more noticeable, with both spoilers generating

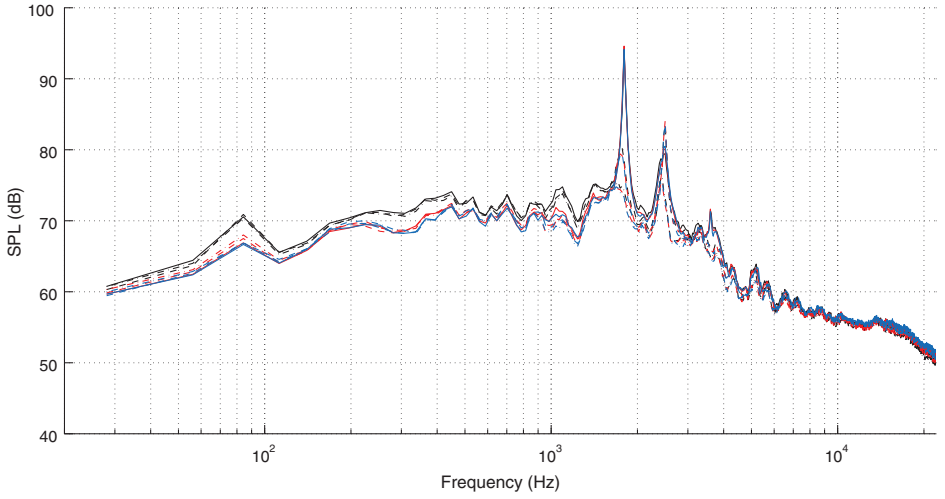

a) Narrowband data for all angles of attack - black lines are the conventional spoiler, blue are for spoiler 3, and red are for spoiler 4

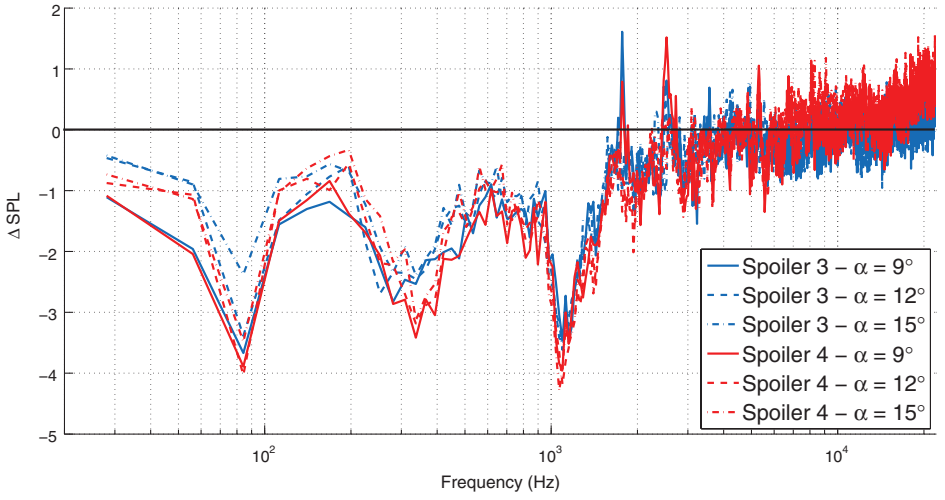

b) Change in SPL for spoiler 3 and 4 for all angles of attack

Fig. 20 Narrowband and difference in SPL of fractal spoilers compared to the conventional spoiler at $\phi = 90$ deg, $U_\infty = 60$ ms^{-1}.

Table 3 Aerodynamic performance of the spoilers on the three-element wing section, for various angles of attack[a]

Spoiler	P_L, %	P_D, %	C_L	C_D	L/D
		$\alpha = 9°$			
Solid	714.74 N	212.94 N	1.04	0.31	3.35
Spoiler 3	0.03	−4.70	1.04	0.30	3.47
Spoiler 4	−0.53	−5.27	1.04	0.30	3.47
		$\alpha = 12°$			
Solid	819.70 N	238.24 N	1.19	0.35	3.40
Spoiler 3	0.78	−2.33	1.21	0.34	3.56
Spoiler 4	−0.51	−4.11	1.19	0.33	3.62
		$\alpha = 15°$			
Solid	918.52 N	267.98 N	1.34	0.39	3.44
Spoiler 3	1.36	−2.14	1.36	0.38	3.58
Spoiler 4	0.69	−2.28	1.35	0.38	3.55

[a]P_L and P_D are the percentage change in the lift and drag forces at $U_\infty = 60$ ms^{-1}, respectively, compared with the solid spoiler (a negative value indicating a percentage decrease). Forces acting on solid spoiler are shown.

more drag force as the wing angle of attack increases, that is, a smaller percentage drop as the angle increases. It is possible that, as the wing angle increases, the effective blockage of the fractal spoilers increases, which is why it could be generating more drag. Nevertheless, the relatively small changes in lift and drag forces generated by the fractal spoilers would make them an ideal replacement to the conventional spoiler, especially for $\alpha = 9$ deg where a 0.03% increase in lift force and a 4.70% decrease in drag is observed for spoiler 3 compared with the solid spoiler.

The lift-to-drag ratio and coefficients of lift and drag are also presented, where the reference area is defined as the frontal area of the wing section, ignoring the porosity of the fractal spoilers. As expected, the coefficients are roughly similar for all configurations because there is very little change in the forces. The lift-to-drag ratio, however, shows an increase for the two fractal spoilers due to the slight reduction in drag force generation.

V. Conclusions

Fractal grids generate bespoke turbulence designed specifically for a particular application which, in this case, is low-noise aircraft spoilers. The turbulence they create can be made to optimally interfere and destroy/modify the large-scale flow structure and, therefore, reduce the low-frequency noise without altering the essential lift/drag characteristics of the spoiler when mounted on a scaled-down A320 wing section. The atmosphere attenuates high-frequency noise faster than low-frequency noise so that the amplified high frequencies of the fractal spoilers may be less of a concern than the low-frequency noise.

It has been shown that a fractal square spoiler can reduce the noise (up to 4 dB), while not affecting the lift and drag characteristics of the wing section that much (the fractal spoilers generating 0.03% more lift force and 4.70% less drag force at a wing angle of 9 deg). At higher angles of wing incidence, namely 15 deg, the change in lift is 1.36%, while generating 2.14% less drag.

Particle image velocimetry measurements have also shown that the fractal spoilers generate a highly intense bleed flow, with increased levels of turbulence intensity, turbulent kinetic energy, and velocity compared with a regular grid spoiler.

The spoiler design used in this paper is by no means an optimal design, and the results presented here should not be considered definitive for all fractal spoilers. Instead, it should be seen as a proof-of-concept design, showing how thickness ratio and distance between the grids appear to affect the acoustic signature of the spoilers. The results suggest that we have relatively high levels of control over the performance of the spoiler by making small alterations to the design, with results suggesting that, by increasing the thickness ratio, we achieve an improvement in sound pressure level across all frequencies, while not changing the blockage ratio. It is believed that, by scaling up the spoiler, there would be fewer mechanical restraints, more flexibility in the design, and the ability to get the same results, if not better.

Acknowledgments

The authors are grateful to Werner Dobrzynski and Michael Pott-Polenske from the DLR Institute at Brunswick for their input and use of Acoustic Wind Tunnel Brunswick for the combined aeroacoustic study of the spoiler. We are grateful to Jean-Paul Bonnet for bringing the Imperial and Poitiers teams together on this project. The research leading to these results has received funding from the European Communities Seventh Framework Programme (FP7/2007-2013) under OPENAIR, grant 34313.

References

[1] Queiros-Conde, D., and Vassilicos, J., "Turbulent Wakes of 3D Fractal Grids," *Workshop on Intermittency in Turbulent Flows and Other Dynamical Systems*, Cambridge Univ. Press, New York, 2001, pp. 136–167.

[2] Staicu, A., Mazzi, B., Vassilicos, J. C., and van de Water, W., "Turbulent Wakes of Fractal Objects," *Physical Review E: Statistical Physics, Plasmas, Fluids, and Related Interdisciplinary Topics*, Vol. 67, No. 6, 2003, p. 66306. doi:10.1103/PhysRevE.67.066306

[3] Hurst, D., and Vassilicos, J. C., "Scalings and Decay of Fractal-Generated Turbulence," *Physics of Fluids*, Vol. 19, No. 3, 2007, p. 035103. doi:10.1063/1.2676448

[4] Seoud, R. E., and Vassilicos, J. C., "Dissipation and Decay of Fractal-Generated Turbulence," *Physics of Fluids*, Vol. 19, No. 10, 2007, p. 105108. doi:10.1063/1.2795211

[5] Mazellier, N., and Vassilicos, J. C., "Turbulence Without Richardson-Kolmogorov Cascade," *Physics of Fluids*, Vol. 22, No. 7, 2010, p. 075101. doi:10.1063/1.3453708

[6] Mazzi, B., and Vassilicos, J. C., "Fractal-Generated Turbulence," *Journal of Fluid Mechanics*, Vol. 502, No. 1, 2004, pp. 65–87. doi:10.1017/S0022112003007249

[7] Nagata, K., Suzuki, H., Sakai, Y., Hayase, T., and Kubo, T., "DNS of Passive Scalar Field with Mean Gradient in Fractal-Generated Turbulence," *Physica Scripta*, Vol. 2008, No. T132, 2008, p. 014054.

[8] Laizet, S., Lamballais, E., and Vassilicos, J. C., "A Numerical Strategy to Combine High-Order Schemes, Complex Geometry and Parallel Computing for High Resolution DNS of Fractal Generated Turbulence," *Computers and Fluids*, Vol. 39, No. 3, 2010, pp. 471–484. doi:10.1016/j.compfluid.2009.09.018

[9] Stresing, R., Peinke, J., Seoud, R. E., and Vassilicos, J. C., "Defining a New Class of Turbulent Flows," *Physical Review Letters*, Vol. 104, No. 19, 2010, p. 194501. doi:10.1103/PhysRevLett.104.194501

[10] Sakaliyski, K. D., Hileman, J. I., and Spakovszky, Z. S., "Aeroacoustics of Perforated Drag Plates for Quiet Transport Aircraft," AIAA Paper 2007-1032, 2007.

[11] Owens, R., "Energy Efficient Engine Performance System—Aircraft Integration Evaluation," NASA CR-159488, 1979.

[12] Tam, C. K. W., "Jet Noise: Since 1952," *Theoretical and Computational Fluid Dynamics*, Vol. 10, No. 1, 1998, pp. 393–405. doi:10.1007/s001620050072

[13] Tam, C., Golebiowski, M., and Seiner, J., "On the Two Components of Turbulent Mixing Noise from Supersonic Jets," AIAA Paper 96-1716, 1996.

[14] Tam, C., and Zaman, K., "Subsonic Jet Noise from Non-axisymmetric and Tabbed Nozzles," *AIAA Journal*, Vol. 38, No. 4, 2000, p. 592–599. doi:10.2514/2.1029

[15] Karabasov, S. A., "Understanding Jet Noise." *Philosophical Transactions, Series A: Mathematical, Physical, And Engineering Sciences*, Vol. 368, No. 1924, 2010, pp. 3593–3608. doi:10.1098/rsta.2010.0086

[16] Dowell, E., "Radiation from Panels as a Source of Airframe Noise," *AIAA Journal*, Vol. 13, No. 11, 1975, pp. 1529–1530. doi:10.2514/3.7027

[17] Dobrzynski, W., and Buchholz, H., "Full-Scale Noise Testing on Airbus Landing Gears in the German-Dutch Wind Tunnel," AIAA Paper 97-1597, 1997.

[18] Dobrzynski, W., Chow, L., Guion, P., and Shiells, D., "A European

Study on Landing Gear Airframe Noise Sources," AIAA Paper 2000-1971, 2000.
[19] Manneville, A., Pilczer, D., and Spakovszky, Z., "Preliminary Evaluation of Noise Reduction Approaches for a Functionally Silent Aircraft," *Journal of Aircraft*, Vol. 43, No. 3, 2006, pp. 836–840. doi:10.2514/1.16424
[20] Castro, I. P., "Wake Characteristics of Two-Dimensional Perforated Plates Normal to an Air-Stream," *Journal of Fluid Mechanics*, Vol. 46, No. 3, 1971, pp. 599–609. doi:10.1017/S0022112071000727
[21] Ranga Raju, K. G., Garde, R. J., Singh, S. K., and Singh, N., "Experimental Study on Characteristics of Flow Past Porous Fences," *Journal of Wind Engineering and Industrial Aerodynamics*, Vol. 29, Nos. 1–3, 1988, pp. 155–163. doi:10.1016/0167-6105(88)90154-7
[22] Shiau, B. S., "Measurement of Turbulence Characteristics for Flow Past Porous Windscreen," *Journal of Wind Engineering and Industrial Aerodynamics*, Vol. 74, No. 1, 1998, pp. 521–530. doi:10.1016/S0167-6105(98)00047-6
[23] Lee, S. J., and Kim, H. B., "Laboratory Measurements of Velocity and Turbulence Field Behind Porous Fences," *Journal of Wind Engineering and Industrial Aerodynamics*, Vol. 80, No. 3, 1999, pp. 311–326. doi:10.1016/S0167-6105(98)00193-7
[24] Fang, F. M., and Wang, D. Y., "On the Flow Around a Vertical Porous Fence," *Journal of Wind Engineering and Industrial Aerodynamics*, Vol. 67, No. 1, 1997, pp. 415–424. doi:10.1016/S0167-6105(97)00090-1
[25] Lighthill, M. J., "On Sound Generated Aerodynamically. I. General Theory," *Proceedings of the Royal Society of London, Series A: Mathematical and Physical Sciences*, Vol. 211, No. 1107, 1952, pp. 564–587. doi:10.1098/rspa.1952.0060
[26] Curle, N., "The Influence of Solid Boundaries upon Aerodynamic Sound," *Proceedings of the Royal Society of London, Series A: Mathematical and Physical Sciences*, Vol. 231, No. 1187, 1955, pp. 505–514. doi:10.1098/rspa.1955.0191
[27] Gerrard, J. H., "Measurements of the Sound from Circular Cylinders in an Air Stream," *Proceedings of the Physical Society, London, Section B*, Vol. 68, No. 7, 1955, p. 453. doi:10.1088/0370-1301/68/7/307
[28] Liow, Y. S. K., Tan, B. T., Thompson, M. C., and Hourigan, K., "Sound Generated in Laminar Flow Past a Two-Dimensional Rectangular Cylinder," *Journal of Sound and Vibration*, Vol. 295, Nos. 1–2, 2006, pp. 407–427. doi:10.1016/j.jsv.2006.01.014
[29] King, W. F., and Pfizenmaier, E., "An Experimental Study of Sound Generated by Flows Around Cylinders of Different Cross-Section," *Journal of Sound and Vibration*, Vol. 328, No. 3, 2009, pp. 318–337. doi:10.1016/j.jsv.2009.07.034

M. Glauser
Associate Editor